Monthly Notices of the ROYAL ASTRONOMICAL SOCIETY

MNRAS **00,** 1 (2026)
Advance Access publication 2026 March 09

https://doi.org/10.1093/mnras/stag462

ExoMol line lists – LXVI. Rotation–vibration line lists for the deuterated ammonia isotopologues $^{14}NH_2D$ and $^{14}ND_2H$

Oleksiy A. Smola,[1] Sergei N. Yurchenko,[1] Jonathan Tennyson,[1]★ Elisabetta Cané,[2] Filippo Tamassia,[2] Kirill Batrakov,[1] Emery Grahill-Bland[1] and Jazz E. Z. Ooi[1]

[1]*Department of Physics and Astronomy, University College London, Gower Street, London WC1E 6BT, UK*
[2]*Dipartimento di Chimica Industriale "Toso Montanari", Università di Bologna, Viale del Risorgimento 4, 40136 Bologna, Italy*

Accepted 2026 March 2. Received 2026 February 23; in original form 2026 January 11

ABSTRACT

We present new CoYuTe rovibrational line lists for the asymmetric deuterated isotopologues of ammonia, $^{14}NH_2D$ and $^{14}ND_2H$. Variational calculations were performed using the TROVE (Theoretical ROVibrational Energies) nuclear motion program, employing newly implemented non-rigid reference frames. The semi-empirical CoYuTe potential energy surface and a high-level *ab initio* dipole moment surface of NH_3 (CCSD(T)/aug-cc-pVQZ) were adopted. The line lists span 0–10 000 cm^{-1} and are applicable at temperatures up to 1000–1500 K. Accuracy was improved through substitution of empirically derived $^{14}NH_2D$ and $^{14}ND_2H$ MARVEL (Measured Active Rotational–Vibrational Energy Levels) energy levels, yielding line positions consistent with available experimental data. The new line lists accurately reproduce existing infrared spectra and, for the first time, provide complete coverage of NH_2D and ND_2H transitions suitable for both cold astrophysical environments and high-temperature exoplanetary and brown dwarf atmospheres. At terrestrial isotopic abundances, NH_2D contributes significantly to atmospheric absorption, highlighting its importance for remote sensing and making it a strong candidate for inclusion in HITRAN (high-resolution transmission molecular absorption database). The line lists and partition functions are available from the ExoMol database at www.exomol.com.

Key words: molecular data – opacity – planets and satellites: atmospheres – stars: atmospheres – ISM: molecules.

1 INTRODUCTION

Partially deuterated isotopologues of ammonia, NH_2D and ND_2H, together with the fully deuterated analogue ND_3, are key molecules in a wide range of astrophysical and planetary environments. They have been detected in star-forming regions, molecular clouds, and hot cores (B. Zuckerman, J. A. Ball & C. A. Gottlieb 1971; E. N. Rodriguez Kuiper, B. Zuckerman & T. B. H. Kuiper 1978; M. Olberg et al. 1985; C. M. Walmsley et al. 1987; S. Tiné et al. 2000; R. Y. Shah & A. Wootten 2001). Because of their enhanced stability at low temperatures, these species serve as important tracers of nitrogen chemistry and deuterium fractionation in cold interstellar clouds and pre-stellar cores (e.g. E. Roueff et al. 2005). Deuterium fractionation is particularly valuable as a diagnostic of physical conditions: the D/H ratios measured in molecules provide constraints on ion–molecule chemistry in the interstellar medium and may retain information about the thermal and chemical history of material incorporated into planetary systems.

Ammonia isotopologues are also of interest in planetary atmospheres. NH_3 plays a major role in the composition and dynamics of the giant planets, where isotopologue abundances can be used to probe nitrogen isotopic ratios, vertical mixing, and disequilibrium chemistry (L. N. Fletcher et al. 2014). Similar considerations are expected to apply to exoplanets, where the detection of NH_2D or ND_2H would provide new constraints on bulk atmospheric composition and isotopic enrichment.

Accurate and comprehensive spectroscopic data for NH_2D and ND_2H are essential for both observational and modelling studies. Infrared spectra of NH_2D and ND_2H have been reported by (L. Coudert, A. Valentin & L. Henry 1986; V. Job et al. 1986, 1987; S. Kartha et al. 1988; M. Snels, H. Hollenstein & M. Quack 2003, 2006a; M. Halonen & L. Halonen 2006) while the visible $5\nu_1$ band of these species was reported by H. Akagi et al. (2005). Experimental data on NH_2D and ND_2H are restricted to limited frequency ranges and near-room-temperature conditions, lacking the coverage needed for high-temperature environments such as brown dwarf and exoplanetary atmospheres. No comprehensive line lists currently exist for these asymmetric deuterated isotopologues.

In this work, we present new variational line lists for $^{14}NH_2D$ and $^{14}ND_2H$, computed using the Theoretical ROVibrational Energies (TROVE) nuclear motion program. The calculations employ the semi-empirical CoYuTe potential energy surface (PES), originally developed for hot $^{14}NH_3$ (P. A. Coles, S. N. Yurchenko & J. Tennyson 2019), together with a high-level *ab initio* CCSD(T)/aug-cc-pVQZ dipole moment surface (DMS). The

★ E-mail: j.tennyson@ucl.ac.uk

Table 1 Spectroscopic state notations used for NH_2D and ND_2H, and their mapping to the corresponding local mode labelling n_1, n_2, n_3, n_4, n_5, and n_6, used for the variational calculations. Associated fundamental band centres in cm^{-1} are taken from M. Snels et al. (2006b). Γ is the symmetry of the vibrational mode in C_{2v}(M).

		NH_2D		ND_2H							
State	Γ	Calc.	Obs.	Calc.	Obs.	n_1	n_2	n_3	n_4	n_5	n_6
g.s.^{s}	A_1	0	0.00	0	0.00	0	0	0	0	0	0
g.s.^{a}	B_1	0.40593	0.41043	0.17074	0.17474	0	0	0	0	0	1
ν_1^s	A_1	2506.509	2506.63	3404.238	3404.43	1	0	0	0	0	0
ν_1^a	B_1	2505.895	2506.09	3404.316	3404.57	1	0	0	0	0	1
ν_2^s	A_1	876.375	875.91	810.227	810.23	0	0	0	0	0	2
ν_2^a	B_1	896.561	896.24	819.565	819.56	0	0	0	0	0	3
ν_{3a}^s	A_1	3365.244	3364.87	2430.799	2430.98	0	0	1	0	0	0
ν_{3a}^a	B_1	3367.589	3367.20	2434.622	2434.81	0	0	1	0	0	1
ν_{3b}^s	B_2	3438.863	3438.99	2559.807	2560.44	0	1	0	0	0	0
ν_{3b}^a	A_2	3439.032	3439.17	2559.963	2560.60	0	1	0	0	0	1
ν_{4a}^s	A_1	1605.640	1605.57	1233.374	1233.39	0	0	0	1	0	0
ν_{4a}^a	B_1	1591.002	1591.06	1235.890	1235.95	0	0	0	1	0	1
ν_{4b}^s	B_2	1389.906	1389.89	1461.794	1461.98	0	0	0	0	1	0
ν_{4b}^a	A_2	1390.495	1390.49	1461.992	1462.20	0	0	0	0	1	1

accuracy of the variationally computed term values has been enhanced by incorporating empirical energies, derived through the Measured Active Rotational–Vibrational Energy Levels (MARVEL) procedure (T. Furtenbacher, A. G. Császár & J. Tennyson 2007) using observed high-resolution spectra (M. T. Weiss & M. W. P. Strandberg 1951; M. Lichtenstein, J. Gallagher & V. Derr 1964; M. J. Kelly, R. E. Francke & M. S. Feld 1970; F. C. De Lucia & P. Helminger 1975; E. Cohen & H. Pickett 1982; M. Bester et al. 1983; L. Coudert et al. 1986; V. Job et al. 1986, 1987; L. Fusina et al. 1988; S. Kartha et al. 1988; M. Snels et al. 2003; C. Endres et al. 2006; M. Halonen & L. Halonen 2006; M. Snels, H. Hollenstein & M. Quack 2006a, b; M. Melosso et al. 2020; E. Canè et al. 2022; F. Tamassia et al. 2025) for the pure rotational, inversional, and the fundamental vibrational bands (ν_1, ν_2, ν_{3a}, ν_{3b} ν_{4a}, ν_{4b}).

We provide complete and systematically validated line lists for the asymmetric deuterated isotopologues of ammonia. They are designed for broad applicability, from modelling the cold environments of interstellar clouds to interpreting high-temperature spectra of exoplanets and brown dwarfs. We further show that $^{14}NH_2D$ contributes significantly to absorption in Earth's atmosphere. The $^{14}NH_2D$ and $^{14}ND_2H$ line lists are provided as part of the ExoMol project (J. Tennyson & S. N. Yurchenko 2012; J. Tennyson et al. 2024b), which already contains line lists for $^{14}NH_3$ (P. A. Coles et al. 2019) and $^{15}NH_3$ (S. N. Yurchenko et al. 2024).

2 QUANTUM NUMBERS AND SELECTION RULES

A clear and consistent labelling scheme is essential for describing the rovibrational states of $^{14}NH_2D$ and $^{14}ND_2H$. Both molecules are quasi-planar, with a relatively low inversion barrier compared to their parent species $^{14}NH_3$, and their rovibrational states can be classified using the irreducible representations of the molecular symmetry group C_{2v}(M) (P. R. Bunker & P. Jensen 1998): A_1, A_2, B_1, and B_2. In spectroscopic practice, the vibrational states of $^{14}NH_2D$ and $^{14}ND_2H$ are usually mapped onto the four fundamental modes of $^{14}NH_3$: the symmetric stretch (ν_1), the symmetric inversion (ν_2), and the asymmetric stretch and bend (ν_3, ν_4). For the asymmetric deuterated isotopologues, however, the degeneracy of the ν_3 and ν_4 modes is lifted, giving rise to independent degrees of freedom, labelled ν_{3a}, ν_{3b} and ν_{4a}, ν_{4b}. In addition, the inversion wavefunction is classified with labels *s* (symmetric) and *a* (antisymmetric), which define its parity with respect to the inversion barrier. The rotational motion of $^{14}NH_2D$ and $^{14}ND_2H$ is described by the asymmetric top quantum numbers J, K_a, K_c, where *a* denotes the axis with the smallest moment of inertia. The spectroscopic classification of the fundamental vibrational states of $^{14}NH_2D$ and $^{14}ND_2H$ is summarized in Table 1 showing their vibrational band labels as well as associated irreducible representations and corresponding local mode quantum numbers used during the variational calculation.

The state-dependent nuclear degeneracy factors, g_{ns}, required for intensity and partition function calculations are as follows: 24 (A_1 and A_2, ortho) and 12 (B_1 and B_2, para) for ND_2H and 9 (A_1 and A_2, para) and 27 (B_1 and B_2, ortho) NH_2D, where ExoMolHD, like high-resolution transmission molecular absorption database (HITRAN), uses the 'physicists' convention which includes the entire nuclear spin degeneracy in g_{ns} (Y. V. Pavlenko, S. N. Yurchenko & J. Tennyson 2020).

The electric-dipole (single-photon) selection rules for NH_2D and ND_2H, derived from C_{2v}(M) symmetry are

$$\Delta J = 0, \pm 1, \quad J' + J'' \neq 0,$$
$$A_1 \leftrightarrow A_2, \quad B_1 \leftrightarrow B_2.$$

3 MARVEL DATA FOR NH_2D AND ND_2H

The coverage of the experimental transition sources on NH_2D and ND_2H used in the MARVEL analysis is listed in Tables 2 and 3; these sources are discussed below.

51WeSt (M. T. Weiss & M. W. P. Strandberg 1951) provided microwave spectra in the 4000–80 000 MHz frequency range for the vibrational ground state of both NH_2D and ND_2H.

64LiGaDe (M. Lichtenstein et al. 1964) measured the microwave absorption of the vibrational ground state in the 80 000–210 000 MHz range for both NH_2D and ND_2H.

70KeFrFe (M. J. Kelly et al. 1970) measured the inversion splitting of three lines in the vibrational ground state of NH_2D.

75LuHe (F. C. De Lucia & P. Helminger 1975) measured 82 inversion–rotation transitions in the range 80–600 GHz using high-resolution microwave techniques for the isotopologues NH_2D and ND_2H.

Table 2 Sources of the MARVEL transitions for NH_2D, their spectral range, number of validated (self-consistent) transitions V out of the total T, and average uncertainty AU.

Segment	Source	Range (cm^{-1})	V/T	AU (cm^{-1})
75LuHe	F. C. De Lucia & P. Helminger (1975)	4.92–17.09	32/32	3.3×10^{-7}
82CoPi	E. Cohen & H. Pickett (1982)	0.25–28.5	108/108	9.2×10^{-7}
83BeUrYaWi	M. Bester et al. (1983)	2.87–3.67	9/9	6.3×10^{-7}
51WeSt	M. T. Weiss & M. W. P. Strandberg (1951)	0.25–2.47	20/20	2.0×10^{-6}
64LiGaDe	M. Lichtenstein et al. (1964)	2.55–6.11	12/12	3.3×10^{-6}
20MeDoGaPu	M. Melosso et al. (2020)	11.1–11.1	1/1	1.4×10^{-5}
06HaHa	M. Halonen & L. Halonen (2006)	1496.28–1739.69	310/317	1.0×10^{-4}
06SnHoQu	M. Snels et al. (2006b)	2392.11–3543.66	889/890	1.0×10^{-4}
22CaDiFuTa	E. Canè et al. (2022)	0.28–399.53	2180/2180	1.2×10^{-4}
86CoVaHe	L. Coudert et al. (1986)	734–1079.87	1018/1022	2.0×10^{-4}
88FuDiJoHa	L. Fusina et al. (1988)	28.76–219.19	259/259	2.5×10^{-4}
06SnHoQua	M. Snels et al. (2006a)	1240.79–1699.5	673/673	1.0×10^{-3}
70KeFrFe	M. J. Kelly et al. (1970)	944.13–970.64	3/3	2.3×10^{-3}
86JoKaKa	V. Job et al. (1986)	745.37–1029.45	616/616	3.0×10^{-3}
21MeBiDoKi	M. Melosso et al. (2021)	2.87–52.13	41/41	2.6×10^{-2}

Table 3 Sources of the MARVEL transitions for ND_2H, their spectral range, number of validated transitions V out of the total T, and average uncertainty AU.

Segment	Source	Range (cm^{-1})	V/T	AU (cm^{-1})
75LuHe	F. C. De Lucia & P. Helminger (1975)	0.16–17.18	66/70	3.3×10^{-7}
06EnMuBrPa	C. Endres et al. (2006)	0.68–203.31	299/299	6.0×10^{-6}
51WeSt	M. T. Weiss & M. W. P. Strandberg (1951)	0.26–2.26	14/14	2.4×10^{-6}
64LiGaDe	M. Lichtenstein et al. (1964)	2.32–7.04	14/14	3.3×10^{-6}
06SnHoQu	M. Snels et al. (2006b)	1150.3–1545.85	843/843	1.8×10^{-4}
88KaSiJoKa	S. Kartha et al. (1988)	866.13–995.89	115/120	1.2×10^{-4}
25TaLoFuCa	F. Tamassia et al. (2025)	65.39–1447.76	6848/6850	4.0×10^{-4}
86CoVaHe	L. Coudert et al. (1986)	733.63–988.53	886/894	3.2×10^{-4}
88FuDiJoHa	L. Fusina et al. (1988)	0.16–219.36	760/761	3.6×10^{-4}
03SnHoQu	M. Snels et al. (2003)	2320.38–3491.16	1655/1655	1.1×10^{-3}
22CaDiFuTa	E. Canè et al. (2022)	0.17–378.23	3201/3201	1.4×10^{-3}
21MeBiDoKi	M. Melosso et al. (2021)	9.91–217.87	748/766	4.9×10^{-2}

82CoPi (E. Cohen & H. Pickett 1982) measured 86 inversion–rotation lines in the 7.5–850 GHz region belonging to the vibrational ground state of NH_2D.

83BeYaWiU (M. Bester et al. 1983) measured both inversion components of the 1_{11}–1_{01} transition in the vibrational ground state of NH_2D.

86CoVaHe (L. Coudert et al. 1986) provide measurements of both inversion components for the inversion fundamental ν_2 of NH_2D and ND_2H using Fourier transform infrared (FTIR) spectrometry.

86JoKaKa (V. Job et al. 1986) used diode laser spectroscopy to measure the symmetric and antisymmetric inversion components of the ν_2 inversion fundamental of NH_2D.

87JoKaSi (V. Job et al. 1987) provide a combined analysis of microwave, FTIR, and diode laser data for the symmetric ν_2^s and antisymmetric ν_2^a inversion fundamental of NH_2D.

88FuDiJoHa (L. Fusina et al. 1988) measured far-infrared spectra of the vibrational ground states of NH_2D and ND_2H in the 17–220 cm^{-1} region.

88KaSiJoKa (S. Kartha et al. 1988) provide the symmetric and antisymmetric inversion components of the ν_2 inversion fundamental of ND_2H, measured with diode laser spectroscopy.

03SnHoQu (M. Snels et al. 2003) provide high-resolution FTIR spectra (at 0.004 cm^{-1} resolution) of the stretching fundamentals ν_1^s, ν_1^a, ν_{3a}^s, ν_{3a}^a, ν_{3b}^s, and ν_{3b}^a of the isotopologue ND_2H.

05AkYoYo (H. Akagi et al. 2005) reported line positions from the $5\nu_1$ vibrational band of NH_2D and ND_2H. These lie beyond the 10 000 cm^{-1} cut-off for the line list and were therefore not included in our analysis.

06EnMuBrPa (C. Endres et al. 2006) measured inversion–rotation transitions in the vibrational ground state of ND_2H in the frequency range between 0.08 and 2.58 THz.

06HaHa (M. Halonen & L. Halonen 2006) measured the symmetric and antisymmetric inversion components of the symmetric bending mode ν_{4a} in NH_2D, using FTIR spectroscopy.

06SnHoQu (M. Snels et al. 2006b) provide FTIR measurements (at 0.004 cm^{-1} resolution) of the ν_1^s, ν_1^a, ν_{3a}^s, ν_{3a}^a, ν_{3b}^s, and ν_{3b}^a stretching excitations of NH_2D.

06SnHoQua (M. Snels et al. 2006a) measured FTIR spectra (at 0.004 and 0.01 cm^{-1} resolution) of the bending fundamentals ν_{4a}^s, ν_{4a}^a, ν_{4b}^s, and ν_{4b}^a for both isotopologues NH_2D and ND_2H.

20MeDoGaPu (M. Melosso et al. 2020) studied three microwave transitions in the vibrational ground state of NH_2D at 86, 110, and 333 GHz, using the Lamb-dip technique. Each transition is hyperfine resolved, so the transition frequency of the three parent transitions is obtained as an intensity-weighted average over the hyperfine components, with the uncertainty determined as the intensity-weighted standard deviation.

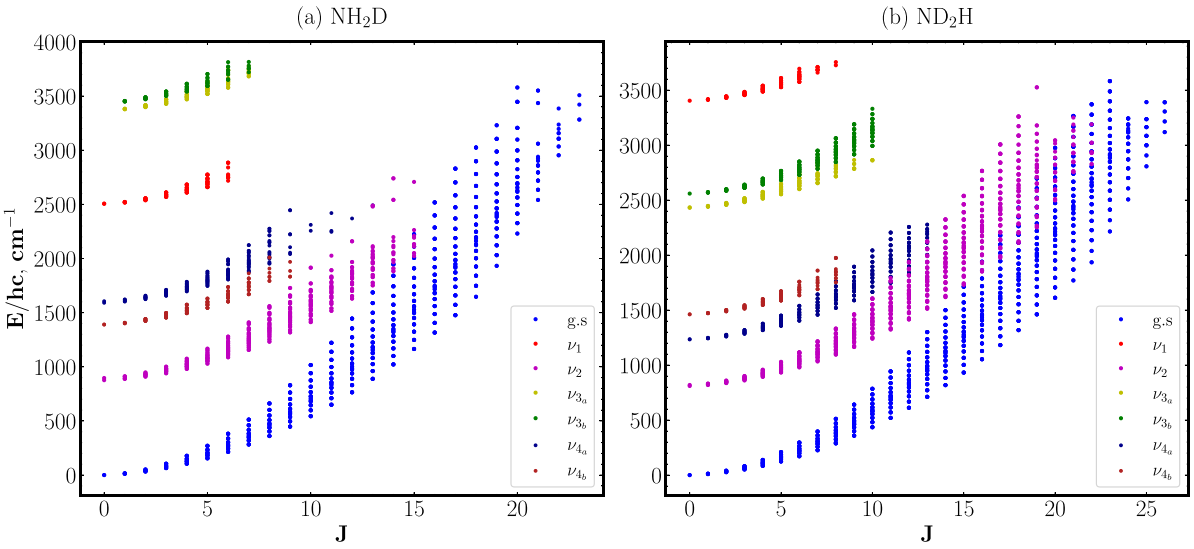

Figure 1. Empirically derived MARVEL energy levels for the isotopologues (a) NH_2D and (b) ND_2H as functions of the rotational quantum number J.

21MeBiDoKi (M. Melosso et al. 2021) measured the hyperfine splitting of lines in the vibrational ground state of NH_2D and ND_2H.

22CaDiFuTa (E. Canè et al. 2022) measured inversion–rotation spectra of the vibrational ground state in the 60–600 cm^{-1} region using a Bruker IFS 125 FTIR spectrometer at a resolution of 0.00096 cm^{-1} for both isotopologues NH_2D and ND_2H.

25TaLoFuCa (F. Tamassia et al. 2025) recorded transitions from the ground state to the ν_2 and ν_{4a} bands, as well as hot rotation–inversion lines within these vibrational states.

The MARVEL (T. Furtenbacher et al. 2007) procedure was applied to the transitions obtained from the literature. Uncertainties were propagated using the bootstrapping algorithm, as available in the MARVEL 4.1 version online (J. Tennyson et al. 2024a). For NH_2D, we invert a network of 6139 experimental transitions to derive 1788 empirical energy levels, while for ND_2H, 15 396 transitions are collected to derive 2987 energy levels. The derived energy levels for both species are illustrated in Fig. 1. To connect ortho and para transition networks, one makes use of so-called magic numbers. For this study, the magic number is chosen to represent the forbidden $0^s_{0,0} \rightarrow 0^a_{0,0}$ transition, whose transition frequency is taken from E. Canè et al. (2022) to be 0.405928 cm^{-1} for NH_2D and 0.170745 cm^{-1} for ND_2H. The uncertainty of the connecting magic number is estimated by taking the average deviation of derived MARVEL term values from those predicted by E. Canè et al. (2022), for the levels $1^a_{0,1}$, $1^s_{1,1}$, and $1^s_{1,0}$ in the case of NH_2D, and the levels $1^s_{0,1}$, $1^a_{1,1}$, and $1^s_{1,0}$ in the case of ND_2H. For NH_2D and ND_2H, the uncertainty is determined to be 1.7×10^{-6} cm^{-1} and 7.0×10^{-6} cm^{-1}, respectively. A further 8 magic numbers for NH_2D and 12 magic numbers for ND_2H are used to connect the largest remaining floating components to the main network, all of which can be found in the MARVEL transitions file in the supplementary data with the segment tag 'MAGIC'.

4 LINE LIST PRODUCTION

Production of high-quality line lists requires (i) a robust nuclear-motion treatment, (ii) accurate potential and DMSs, and (iii) careful state labelling compatible with spectroscopic conventions. In what follows, we outline the TROVE setup used for $^{14}NH_2D$ and $^{14}ND_2H$, the non-rigid reference frames implemented for the large-amplitude inversion motion, the basis set construction and symmetry adaptation, and the generation and MARVEL-based refinement of the final line lists.

4.1 Variational calculation

Line lists for NH_2D and ND_2H were generated with the variational code TROVE (S. N. Yurchenko, W. Thiel & P. Jensen 2007). TROVE employs a kinetic energy operator (KEO) represented as a Taylor-type expansion around a non-rigid reference configuration. For this work, the KEO was expanded to sixth order in five rectilinear linearized coordinates,

$$\xi_i^{\rm lin} = \{\Delta r_1^{\rm lin}, \Delta r_2^{\rm lin}, \Delta r_3^{\rm lin}, S_A^{\rm lin}, S_B^{\rm lin}\},$$

about a large-amplitude coordinate ρ that follows the Hougen–Bunker–Johns formulation (J. T. Hougen, P. R. Bunker & J. W. C. Johns 1970). The linearized coordinates are constructed using the following five combinations of valence coordinates, bond lengths r_1, r_2, and r_3 and interbond angles α_{12}, α_{13}, and α_{23}:

$$\Delta r_1 = r_1 - r_{\rm e}, \quad \Delta r_2 = r_2 - r_{\rm e}, \quad \Delta r_3 = r_3 - r_{\rm e}, \tag{1}$$

$$S_A = \tfrac{1}{\sqrt{6}}(2\alpha_{23} - \alpha_{13} - \alpha_{12}), \quad S_B = \tfrac{1}{\sqrt{2}}(\alpha_{13} - \alpha_{12}), \tag{2}$$

where $r_{\rm e}$ is the equilibrium bond length. The sixth coordinate ρ describes the inversion (umbrella) motion and is defined as the angle between the molecular trisector and any one of the bonds with $\rho = \pi/2$ corresponding to the planar configuration. For NH_2D, the equivalent nuclei are H_2 and H_3; for ND_2H, they are D_2 and D_3.

Defining the Wang functions for rigid-rotor wavefunctions as $|J, k\rangle$, where k is the projection of the rotational angular momentum on the molecular z and the projection on the laboratory Z axes, usually denoted m, is neglected, then the rotational motion is treated by first forming symmetric and antisymmetric combinations (S. N. Yurchenko et al. 2005):

$$|J, 0, \tau_{\rm rot}\rangle, \quad \tau_{\rm rot} = J \bmod 2, \tag{3}$$

Table 4 Rotational symmetry and (K_a, K_c) parity in C_{2v}(M) for NH_2D and ND_2H. Here e/o denote even/odd integers.

Γ_{rot}	τ_{rot}	K_a parity	K_c parity
		NH_2D	
A_1	0	e	e
A_2	1	e	o
B_1	1	o	o
B_2	0	o	e
		ND_2H	
A_1	0	e	e
A_2	1	o	o
B_1	1	o	e
B_2	0	e	o

$$|J, K, \tau_{rot}\rangle = \frac{1}{\sqrt{2}}\Big(|J, |k|\rangle + (-1)^{J+K+\tau_{rot}}|J, -|k|\rangle\Big), \quad \tau_{rot} = 0, 1, \tag{4}$$

with $K = |k|$. Here, τ_{rot} is the associated rotational parity and Γ_{rot} is the irrep in the C_{2v}(M) symmetry group and m is omitted for simplicity. Symmetry adaptation to C_{2v}(M) is carried out as described below; the correspondence between Γ_{rot}, τ_{rot}, and (K_a, K_c) is summarized in Table 4.

All rovibrational eigenfunctions are constructed to transform as irreducible representations of C_{2v}(M) and are labelled accordingly; the correlation with spectroscopic (HITRAN style) labels is illustrated for the fundamentals in Table 1.

For each eigenfunction, TROVE coefficients in the symmetric-top basis are analysed to identify the dominant $|J, K\rangle$ contribution(s). The rotational frame in TROVE is chosen as illustrated in Fig. 2 with the z-axis in the symmetry σ_v plane. The axis frame of type III is used to correlate the TROVE rotational quantum numbers K and associated C_{2v}(M) symmetry to the spectroscopic rotational quantum numbers K_a and K_c following the standard asymmetric-top rules (see e.g. P. R. Bunker & P. Jensen 1998) for NH_2D and ND_2H are given in Table 4.

4.2 Non-rigid reference frames and molecular axes

The vibrational coordinate system follows that used for NH_3. The body-fixed frame xyz satisfies the Eckart–Sayvetz conditions (G. O. Sørensen 1979). For the large-amplitude inversion motion, we employ non-rigid reference frames whose orientation depends on ρ and is defined by principal axis system (PAS) conditions (mass-dependent). The PAS was constructed numerically while maintaining continuity across the inversion pathway; care was taken to handle potential axis flips. Fig. 2 shows the dependence of the rotational constants B_x, B_y, B_z on ρ, and Fig. 3 illustrates the non-rigid frames implemented for NH_2D and ND_2H. Close to planarity, the NH_2D frame correlates to the representation type III, while the ND_2H frame to the representation type II (P. R. Bunker & P. Jensen 1998).

4.3 TROVE basis set and Hamiltonian representation

The 1D primitive vibrational basis functions $\phi_{n_i}(\xi_i^{lin})$ for the three stretches were computed with the Numerov–Cooley method (B. Noumeroff 1923; J. W. Cooley 1961) on a grid spanning 0.4–2.0 Å. For the two asymmetric bends, we used harmonic-oscillator functions; the inversion basis was generated on a finer ρ grid using the Numerov–Cooley method. The stretching bases covered $n_i = 0, \ldots, 9$; bending excitations up to $n_4, n_5 = 16$; inversion up to $n_6 = 36$.

4.4 Contracted basis set and symmetrization

In TROVE rovibrational calculations, a two-step contraction was employed (S. N. Yurchenko, A. Yachmenev & R. I. Ovsyannikov 2017; S. Yurchenko 2023). Three reduced Hamiltonians were first diagonalized for (i) stretches, (ii) bends, and (iii) inversion:

$$\hat{H}^{(1)}_{str}(\xi^{lin}_{1..3}) = \langle 0_4 0_5 0_6|\hat{H}^{6D}|0_6 0_5 0_4\rangle, \tag{5}$$
$$\hat{H}^{(2)}_{bnd}(\xi^{lin}_{4,5}) = \langle 0_1 0_2 0_3 0_6|\hat{H}^{6D}|0_6 0_3 0_2 0_1\rangle, \tag{6}$$
$$\hat{H}^{(3)}_{inv}(\rho) = \langle 0_1 0_2 0_3 0_4 0_5|\hat{H}^{6D}|0_5 0_4 0_3 0_2 0_1\rangle. \tag{7}$$

Eigenfunctions were symmetry adapted to C_{2v}(M). The final vibrational basis is a direct product of the three subspaces, truncated by the polyad

$$P = 4(n_1 + n_2 + n_3) + 2(n_4 + n_5) + n_6 \leq P_{max} = 36.$$

The $J = 0$ eigenfunctions were then truncated using an energy threshold $\tilde{E}_i \leq 18\,000\,cm^{-1}$ and combined with the Wang rotational functions from equations (3), and (4) to form rovibrational bases for $J = 0$–40. For each J, four C_{2v}(M) block Hamiltonians (A_1, A_2, B_1, B_2) were constructed and diagonalized. This contraction strategy yields substantial efficiency gains with negligible loss of accuracy.

4.5 Potential energy surface

Variational calculations used the CoYuTe PES, originally developed for $^{14}NH_3$ and described by P. A. Coles et al. (2018). CoYuTe combines high-level *ab initio* data (MRCI with aug-cc-pwCVQZ/aug-cc-pwCV5Z extrapolated to the CBS limit) with empirical refinement to MARVEL energies of $^{14}NH_3$, and provides an accurate description of the inversion motion. For NH_2D and ND_2H, the PES has proven a reliable foundation for rovibrational energies across a wide temperature range.

4.6 Dipole moment surface

Transition intensities were computed using the same high-level *ab initio* DMS employed in the CoYuTe $^{14}NH_3$ line list (P. A. Coles et al. 2019). Dipole components were calculated at the CCSD(T)/aug-cc-pVQZ level and represented analytically in curvilinear internal coordinates to ensure smooth interpolation over the relevant configuration space.

4.7 Rovibrational line lists: states, transitions, and accuracy refinement

Using this procedure and the CoYuTe spectroscopic model (PES and DMS), CoYuTe line lists for $^{14}NH_2D/^{14}ND_2H$ were generated, consisting of 1766 049 359/4791 272 445 transitions and 4968 160/6829 277 states. Rovibrational states are labelled by $\{J, K_a, K_c; n_1, \ldots, n_6; \Gamma_{vib}, \Gamma_{rot}\}$. For spectroscopic usage, we also provide normal-mode labels $(v_1, v_2, v_{3a}, v_{3b}, v_{4a}, v_{4b}, a/s)$ reconstructed from the local indices. Assignments follow the 'largest coefficient' criterion in the underlying basis, with parity and symmetry checks as constraints (Table 4).

Einstein A coefficients were computed from the DMS to generate transitions up to 10 000 cm^{-1}. The lower state energy cut-off

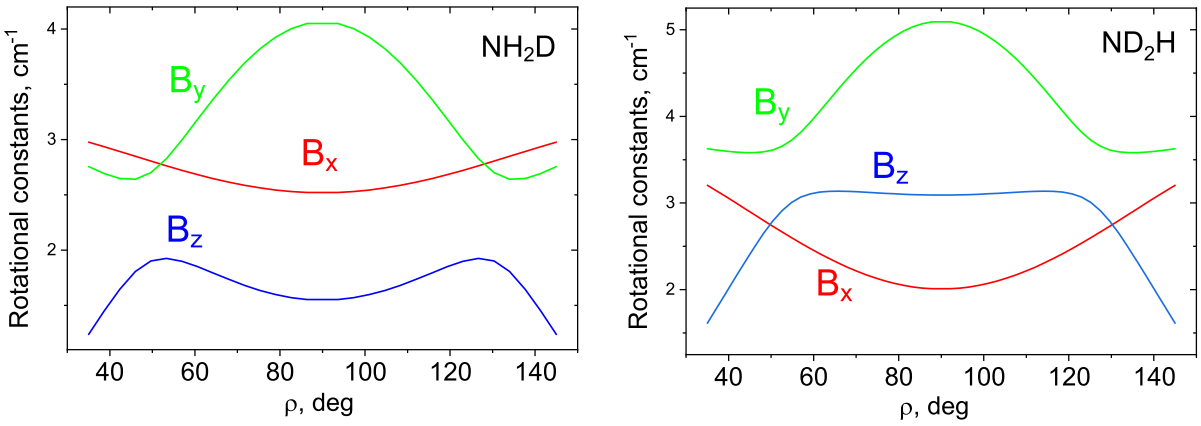

Figure 2. Rotational constants B_x, B_y, B_z as functions of the non-rigid reference coordinate ρ for NH_2D (left) and ND_2H (right).

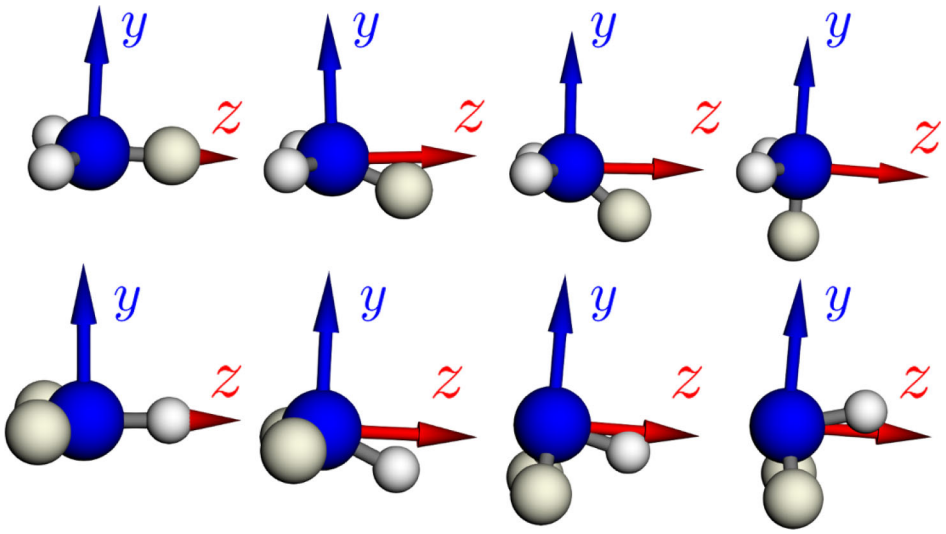

Figure 3. Non-rigid reference molecular frames used for NH_2D (upper) and ND_2H (lower).

was set to $\tilde{E}''_{\rm max} = 6000\,{\rm cm}^{-1}$. We recommend application of the present lists up to about 1000 K (see more on the temperature coverage below).

The calculation accuracy is illustrated in Fig. 4 as observed minus calculated (obs. − calc.) residuals of the term values as a function of J. The quality of the ND_2H energies is significantly affected by the isotope mass substitution, much more than that of NH_2D. For ND_2H, there is a strong dependence on the rotational quantum number K_a with the obs. − calc. residuals growing approximately quadratically.

To improve line positions, variational term values were replaced by empirical energies where available using the MARVEL approach (T. Furtenbacher et al. 2007). This 'MARVELization' significantly enhances internal consistency and agreement with the experiment.

5 LINE LISTS

The NH_2D and ND_2H data sets follow the standard ExoMol format (J. Tennyson, C. Hill & S. N. Yurchenko 2013): each line list comprises a `.states` file (rovibrational term values and quantum numbers), a set of `.trans` files (Einstein A and state indices), and a partition function file `.pf`. Example excerpts are shown in Tables 5 and 6. The `.states` file lists, for each i: the term value $\tilde{E}_i$ ($\rm cm^{-1}$), total degeneracy g_i, J, energy uncertainty, lifetime τ, total symmetry $\Gamma_{\rm tot} \in \{A_1, A_2, B_1, B_2\}$ (C_{2v}(M)), vibrational assignments in both normal mode notation ($v_1, v_2, v_{3a}, v_{3b}, v_{4a}, v_{4b}$) with inversion s/a, and TROVE local indices ($n_1, \ldots, n_6$), as well as rotational labels (K_a, K_c) and $\Gamma_{\rm rot}$. The `Label` field indicates the energy provenance: MARVEL (`Ma`) or calculated (`Ca`) (L. K. McKemmish et al. 2024). The final column preserves the original calculated energy for traceability. The `.trans` files provide the upper/lower state indices (f, i) and Einstein A coefficients ($\rm s^{-1}$); the full transition set is split into wavenumber bins for practicality.

For the uncertainties of the 'MARVELized' energy term values, the experimental (MARVEL) values were used. For calculated energy term values, we assumed uncertainties to be linearly proportional to the assigned normal mode quantum numbers and quadratically proportional to the rotational quantum numbers J and K_a as follows:

$$\text{unc.} = a(v_1 + v_2 + v_{3a} + v_{3b} + v_{4a} + v_{4b}) + bJ(J+1) + cK_a^2,$$

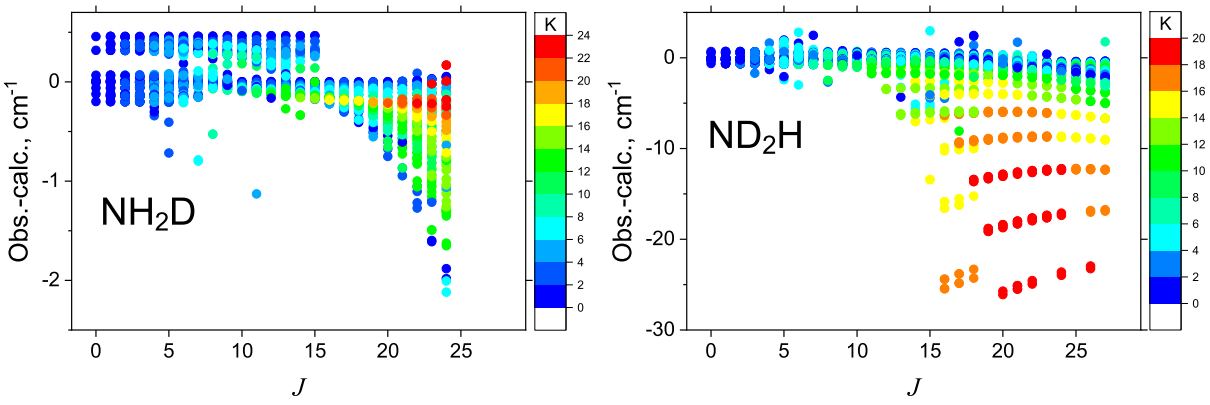

Figure 4. Observed minus calculated (obs. − calc.) values of term values (cm^{-1}) of NH_2D (left) and ND_2H (right) as a function of J. The colour scales are for the rotational $K \equiv K_a$ values.

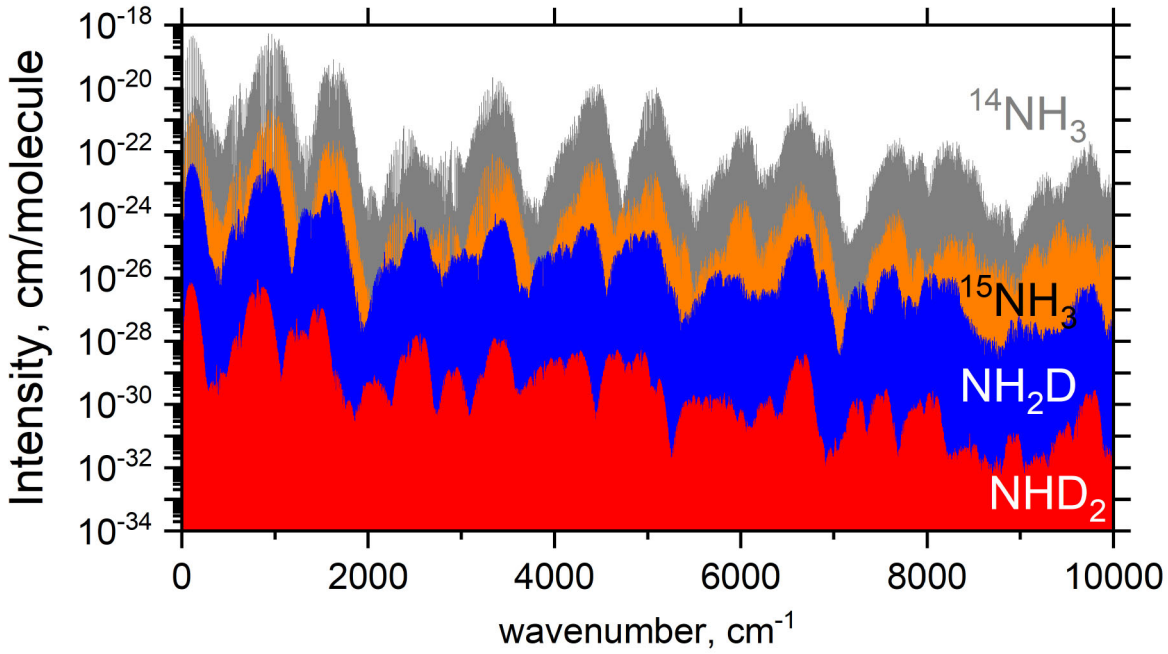

Figure 5. Room temperature ($T = 296$ K) absorption spectra of $^{14}NH_3$ (from P. A. Coles et al. 2019), $^{15}NH_3$ (from S. N. Yurchenko et al. 2024), NH_2D, and ND_2H, each scaled by their natural (terrestrial) isotopic abundances (I. E. Gordon et al. 2022). The plot highlights the relative spectroscopic contributions of the four isotopologues under Earth's atmospheric conditions.

where $a = 0.2$ cm^{-1}, $b = 0.005$ cm^{-1}, $c = 0.2$ cm^{-1} (NH_2D), and $c = 0.6$ cm^{-1} (ND_2H).

Fig. 5 illustrates the relative terrestrial spectroscopic importance of the four isotopologues of ammonia, NH_2D and ND_2H, $^{14}NH_3$ (P. A. Coles et al. 2019), and $^{15}NH_3$ (S. N. Yurchenko et al. 2024), by showing their room temperature absorption spectra with intensities scaled by their natural (terrestrial) abundances (I. E. Gordon et al. 2022).

5.1 Partition functions

Partition functions for NH_2D and ND_2H were computed by direct summation on a 1 K grid from 0 to 2000 K:

$$Q(T) = \sum_i g_{\rm ns}^{(i)}(2J_i+1)\exp\left(-\frac{c_2\tilde{E}_i}{T}\right),$$

where $g_{\rm ns}^{(i)}$ is the nuclear-spin statistical factor, J_i is the rotational quantum number, c_2 is the second radiation constant (cm K), and $\tilde{E}_i$ is the energy relative to the ground state. Fig. 6 shows $Q(T)$ for both isotopologues; NH_2D is compared with the total internal partition sums (TIPS) 2024 value (R. R. Gamache et al. 2025). Agreement is good up to ∼500 K; at higher T, the two curves diverge, likely reflecting differences in underlying state completeness or modelling assumptions. Convergence of the CoYuTe sum with respect to rotational excitation is illustrated at $T = 2000$ K: by $J_{\rm max} = 40$, $Q(T)$ is converged within ≈0.1 per cent, indicating that in terms of $J_{\rm max}$ the present partition functions are sufficiently complete up to 2000 K. Similar vibrational convergence tests of imposed by the lower energy cut-off of 6000 cm^{-1} showed completeness of the partition functions (and therefore of the line lists) to within 2 per cent for $T = 1000$ K. We therefore

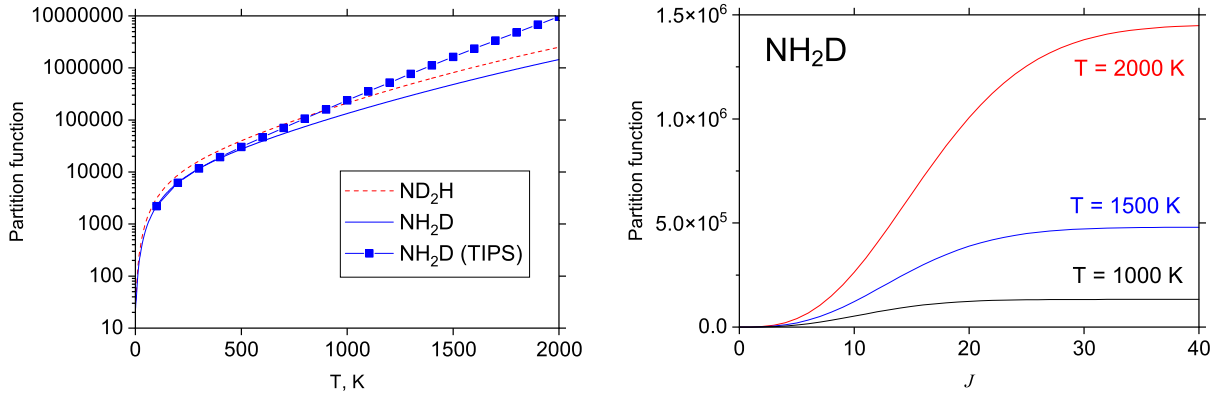

Figure 6. Left: The partition function of NH_2D and ND_2H (CoYuTe) compared to the TIPS 2024 partition function of NH_2D (R. R. Gamache et al. 2025) (squares). Right: Convergence of the partition function of NH_2D as a function of J for $T = 1000$ K, $T = 1500$ K, and $T = 2000$ K.

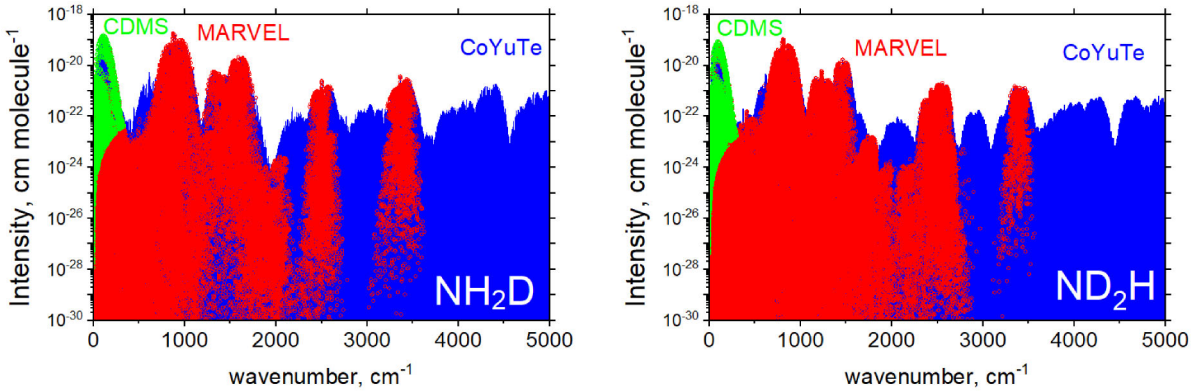

Figure 7. Room temperature ($T = 296$ K) absorption spectra of NH_2D and ND_2H computed using the new CoYuTe line lists (scaled to natural abundance), 1321 662 and 1588 845 lines, respectively, and overlaid with the CDMS (C. P. Endres et al. 2016) (green circles) and MARVEL (red circles) transitions. CDMS (C. P. Endres et al. 2016) data, 3291 and 3644 lines, respectively, cover the ground state rotation–inversion transitions only. The MARVEL data indicate 37 201 and 17 119 CoYuTe transitions generated from the accurate (MARVELized) states only.

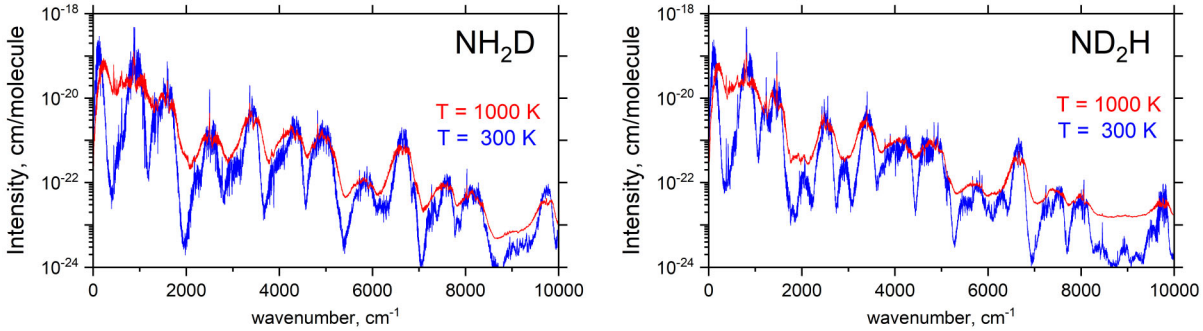

Figure 8. Absorption cross-sections of NH_2D and ND_2H at $T = 296$ K (blue) and $T = 1000$ K (red), illustrating the effect of temperature on the spectra. At elevated temperatures, hot-band transitions from thermally populated excited states fill the gaps between fundamentals and overtones, raising the spectral baseline, while the peak intensities of the fundamentals decrease due to reduced ground-state population. A Gaussian line profile was used with a resolution of 1 cm^{-1}.

recommend the line lists reported for applications up to ∼1000–1500 K. We are therefore puzzled by the disagreement with TIPS for NH_2D at $T > 500$ K.

Fig. 7 summarizes the coverage of transitions anchored to empirical energies (MARVELized) at $T = 296$ K and contrasts this with the full CoYuTe predictions above an intensity threshold of 10^{-30} cm molecule^{-1}. For the microwave region, available Cologne Database for Molecular Spectroscopy (CDMS) data (C. P. Endres et al. 2016) are also included for comparison. This comparison highlights both the experimentally constrained subset and the additional predictive reach of the present line lists across the infrared.

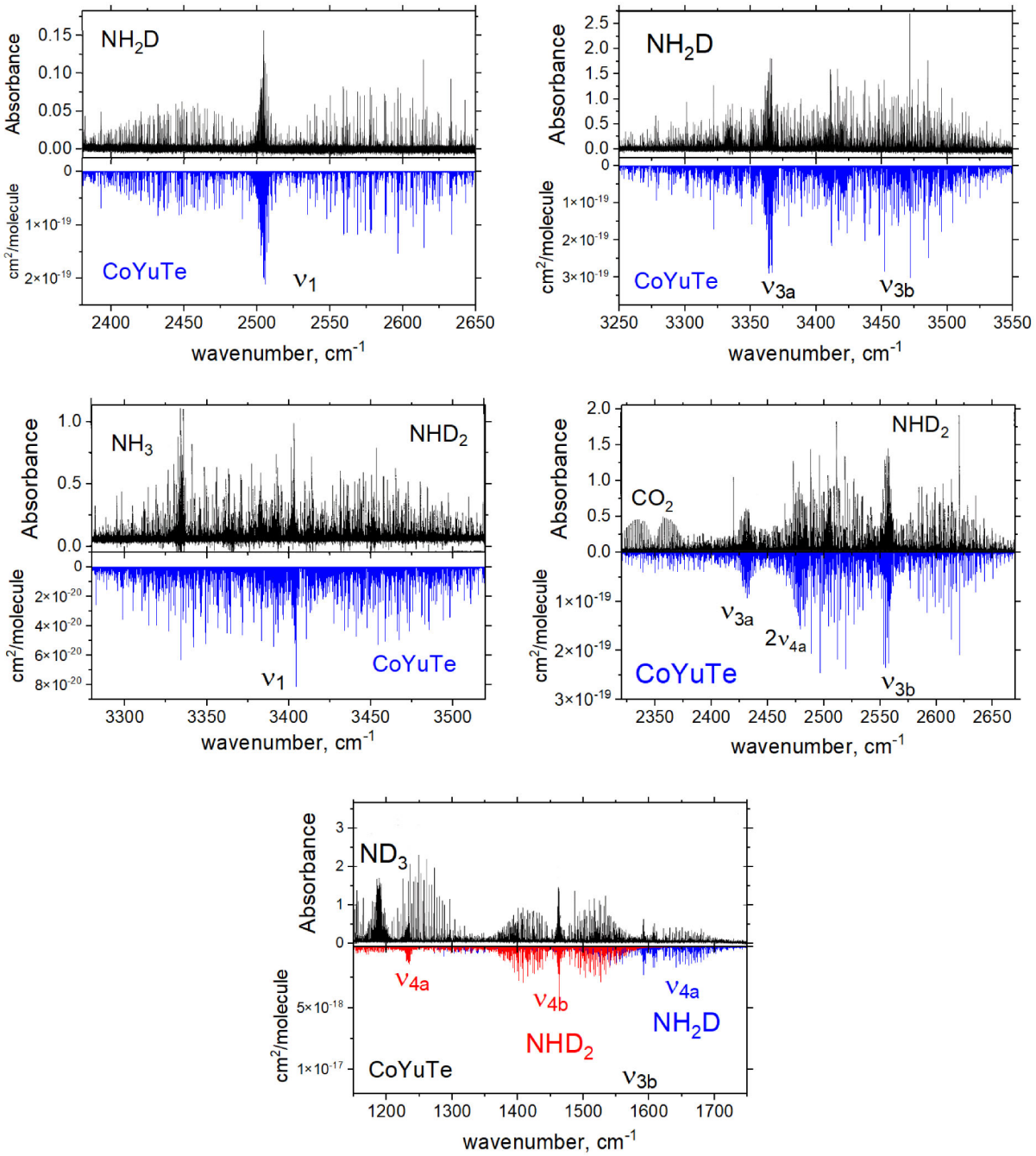

Figure 9. Absorption cross-sections of NH_2D and ND_2H at $T = 296$ K computed using the CoYuTe line lists compared with the experimental spectra of M. Snels et al. (2003, 2006a, b). A Doppler line profile was used with a resolution of 0.01 cm^{-1}. The comparison is qualitative since only published plots, rather than numerical experimental data, were available, but nevertheless shows excellent consistency in both line positions and intensities.

6 ILLUSTRATIONS

The temperature dependence of the NH_2D and ND_2H spectra is illustrated in Fig. 8, which compares absorption cross-sections at $T = 300$ K and $T = 2000$ K. Raising the temperature leads to the progressive filling of gaps between the fundamentals and overtone bands by hot-band transitions, thereby lifting the spectral troughs. At the same time, the peak intensities of the fundamentals and overtones are reduced due to the decreased relative population of the vibrational ground state. This behaviour is characteristic of polyatomic molecules at elevated temperatures and demonstrates the expected redistribution of spectral intensity with increasing thermal excitation.

A more detailed comparison with experiment is presented in Fig. 9, where calculated spectra of NH_2D and ND_2H at $T = 296$ K are compared to the laboratory measurements of M. Snels et al. (2003, 2006a, b) in the ν_1, ν_{3a}, ν_{3b}, ν_{4a}, ν_{4b}, and $2\nu_{4a}$ bands. The agreement in both line positions and intensities is excellent, confirming the reliability of the line lists for spectroscopic analysis. These results also demonstrate the utility of the new data in assisting with experimental line assignments, particularly in crowded spectral regions or at higher excitations where labo-

Table 5 Extract from the `.states` file of the NH_2D line list.

i	$\tilde{E}$/cm^{-1}	g	J	unc/cm^{-1}	τ/s	$\Gamma_{\rm tot}$	v_1	v_2	v_{3a}	v_{3b}	v_{4a}	v_{4b}	s/a	$\Gamma_{\rm vib}$	K_a	K_c	$\Gamma_{\rm rot}$	$\lvert C_i^2\rvert$	n_1	n_2	n_3	n_4	n_5	n_6	Label	$\tilde{E}_{\rm calc.}$/cm^{-1}
1	0.000000	9	0	0.000001	Inf	A1	0	0	0	0	0	0	s	A1	0	0	A1	1.00	0	0	0	0	0	0	Ma	0.000000
2	876.371228	9	0	0.003000	8.9704E-02	A1	0	1	0	0	0	0	s	A1	0	0	A1	1.00	0	0	0	0	0	2	Ma	875.914269
3	1509.901776	9	0	0.400000	6.9613E-02	A1	0	2	0	0	0	0	s	A1	0	0	A1	1.00	0	0	0	0	0	4	Ca	1509.901776
4	1605.639964	9	0	0.000100	1.3427E-01	A1	0	0	1	0	0	0	s	A1	0	0	A1	1.00	0	0	0	1	0	0	Ma	1605.572332
5	2179.508197	9	0	0.600000	4.2478E-02	A1	0	3	0	0	0	0	s	A1	0	0	A1	1.00	0	0	0	0	0	6	Ca	2179.508197
6	2469.865765	9	0	0.400000	5.6974E-02	A1	0	1	1	0	0	0	s	A1	0	0	A1	1.00	0	0	0	1	0	2	Ca	2469.865765
7	2506.505796	9	0	0.000100	3.9554E-01	A1	1	0	0	0	0	0	s	A1	0	0	A1	1.00	1	0	0	0	0	0	Ma	2506.627642
8	2771.004651	9	0	0.400000	3.0530E-01	A1	0	0	0	0	0	2	s	A1	0	0	A1	1.00	0	0	0	0	2	0	Ca	2771.004651
9	3049.101030	9	0	0.600000	3.9195E-02	A1	0	2	1	0	0	0	s	A1	0	0	A1	1.00	0	0	0	1	0	4	Ca	3049.101030
10	3151.400404	9	0	0.800000	3.1817E-02	A1	0	4	0	0	0	0	s	A1	0	0	A1	1.00	0	0	0	0	0	8	Ca	3151.400404
11	3194.133614	9	0	0.400000	5.6872E-02	A1	0	0	2	0	0	0	s	A1	0	0	A1	1.00	0	0	0	2	0	0	Ca	3194.133614
12	3364.866531	9	0	0.200000	1.5425E-01	A1	0	0	1	0	0	0	s	A1	0	0	A1	1.00	0	1	0	0	0	0	Ca	3364.866531
13	3412.160102	9	0	0.400000	5.9920E-02	A1	1	1	0	0	0	0	s	A1	0	0	A1	1.00	1	0	0	0	0	2	Ca	3412.160102

i:	state identifier;
$\tilde{E}$:	state term value;
g:	state degeneracy;
J:	state rotational quantum number;
unc.:	energy uncertainty;
τ:	lifetime;
$\Gamma_{\rm tot}$:	total symmetry in $\mathcal{C}_{2v}$(M);
$v_1, v_2, v_{3a}, v_{3b}\, v_{4a}, v_{4b}$:	normal mode vibrational quantum numbers;
s/a:	inversion symmetry;
$\Gamma_{\rm vib}$:	symmetry of vibrational contribution in $\mathcal{C}_{2v}$(M);
K_a :	rotational quantum number;
K_c :	rotational quantum number;
$\Gamma_{\rm rot}$:	symmetry of rotational contribution in $\mathcal{C}_{2v}$(M);
$\lvert C_i^2\rvert$:	largest coefficient used in the assignment;
$n_1 - n_6$:	TROVE vibrational quantum numbers;
Label:	label indicating if the term value is based on the MARVEL (‘Ma’) isotope extrapolation (‘IE’) or the CoYuTe energy list (‘Ca’);
$\tilde{E}_{\rm calc.}$:	original CoYuTe state term value.

Table 6 Extract from a `.trans` file of the NH_2D CoYuTe line list.

f	i	A_{fi}
4274094	4300204	7.4466e-16
1602946	1650709	2.3016e-16
2799211	2752947	2.6329e-15
1371027	1325721	3.4690e-16
1937548	1889355	3.4061e-16
2705837	2658683	2.7066e-16
1060674	1104081	5.1314e-16
595074	631277	3.1906e-16

Notes. f: upper state counting number;
i: lower state counting number;
A_{fi}: Einstein A coefficient (in s^{-1}).

ratory measurements are more challenging. We note, however, that the comparisons are necessarily qualitative, as only digitized spectra from the original publications were available rather than the underlying experimental line lists. Besides, the $2\nu_{4a}$ band though observed has not been analysed, to the best of our knowledge.

7 CONCLUSIONS

We present new comprehensive variational CoYuTe line lists for the asymmetric deuterated isotopologues of ammonia, $^{14}NH_2D$ and $^{14}ND_2H$, generated with the TROVE nuclear motion program. The calculations employed the high-accuracy CoYuTe PES, originally developed for hot $^{14}NH_3$, together with a high-level *ab initio* DMS. To improve accuracy, empirically derived energy levels from the MARVEL procedure were incorporated, replacing calculated term values where available.

The resulting line lists cover the wavenumber range 0–10 000 cm^{-1} and are reliable for modelling spectra at temperatures up to ∼1000 K, making them suitable for a wide variety of astrophysical and atmospheric applications. Partition functions and temperature-dependent opacities have also been computed and made available. Comparisons with existing experimental data, particularly infrared spectra from the literature, show excellent agreement in both line positions and intensities, lending confidence to the predictive capability of the line lists.

For the first time, complete and systematically generated rovibrational data are now available for NH_2D and ND_2H, filling a long-standing gap in spectroscopic databases. These data are directly relevant for studies of deuterium chemistry in the interstellar medium and star-forming regions, as well as for modelling the atmospheres of planets and brown dwarfs, where ammonia isotopologues may contribute to the opacity. In addition, we find that NH_2D makes a non-negligible contribution to terrestrial atmospheric absorption, strengthening the case for its inclusion in databases such as HITRAN.

All line lists, together with partition functions, are provided in the ExoMol format via www.exomol.com. These resources extend the ExoMol database to cover deuterated ammonia, thereby enabling more complete and accurate modelling of nitrogen chemistry in a range of astrophysical and planetary environments. We also expect this work to provide data that contribute to studies investigating how machine learning techniques can be applied to predict isotopologue extrapolated energy levels in molecules, as have been applied to isotopologues of CO_2 and CO (M. G. Barnfield et al. 2026). Indeed, with a substantially larger data set for ND_2H compared to that of NH_2D, it will be illuminating to study whether energies can be accurately extrapolated from a less abundant isotopologue to a more abundant one.

By combining the CoYuTe PES with the high-accuracy DMS, the present line lists provide comprehensive and precise spectroscopic data for NH_2D and ND_2H, suitable for applications in astrophysical, atmospheric, and laboratory studies. These data sets provide the most complete spectroscopic resource to date for deuterated ammonia.

ACKNOWLEDGEMENTS

This work was supported by the STFC Project No. ST/Y001508/1. The authors acknowledge the use of the UCL Legion High Performance Computing Facility (Legion@UCL) and associated support services in the completion of this work, along with the Cambridge Service for Data Driven Discovery (CSD3) and the DiRAC Data Intensive service DIaL2.5 at the University of Leicester, managed on behalf of the STFC DiRAC HPC Facility (www.dirac.ac.uk). These DiRAC services were funded by BEIS, UKRI and STFC capital funding, and STFC operations grants. DiRAC is part of the UKRI Digital Research Infrastructure. This work was also supported by the European Research Council (ERC) under the European Union's Horizon 2020 Framework Programme through an Advanced Grant number 883830. The authors would like to extend their thanks to all the students at Newham Collegiate Sixth Form, who helped with the MARVEL project for $^{14}ND_2H$, as well as to Serena Maugeri, who helped organize the class as part of the ORBYTS outreach project.

The MARVEL input (transitions) and output (energy) files used in this work, together with the associated 'segment' files for both isotopologues, are provided as part of this paper. The line lists for $^{14}NH_2D$ and $^{14}ND_2H$, together with the associated partition functions and spectroscopic models (including the full set of TROVE input files), are freely available from the ExoMol database at www.exomol.com. The spectroscopic models define the potential and dipole moment expansions, coordinate systems, basis set specifications, and computational ranges, ensuring full reproducibility of the results. The codes used in this work, namely TROVE and EXOCROSS, are freely available via https://github.com/exomol.

DATA AVAILABILITY

The data underlying this article are available in the article, in its online supplementary material, or on the ExoMol website.

REFERENCES

Akagi H., Yokoyama K., Yokoyama A., Wada A., 2005, J. Mol. Spectrosc., 231, 37
Barnfield M. G., Polyansky O. L., Yurchenko S. N., Tennyson J., 2026, J. Mol. Spectrosc.
Bester M., Yamada K., Winnewisser G., Urban S., 1983, A&A, 121, L13
Bunker P. R., Jensen P., 1998, Molecular Symmetry and Spectroscopy, 2nd edn. NRC Research Press, Ottawa
Canè E., Di Lonardo G., Fusina L., Tamassia F., Predoi-Cross A., 2022, J. Mol. Spectrosc., 384, 111581
Cohen E., Pickett H., 1982, J. Mol. Spectrosc., 93, 83
Coles P. A., Ovsyannikov R. I., Polyansky O. L., Yurchenko S. N., Tennyson J., 2018, J. Quant. Spectrosc. Radiat. Transf., 219, 199
Coles P. A., Yurchenko S. N., Tennyson J., 2019, MNRAS, 490, 4638
Cooley J. W., 1961, Math. Comput., 15, 363

Coudert L., Valentin A., Henry L., 1986, J. Mol. Spectrosc., 120, 185
De Lucia F. C., Helminger P., 1975, J. Mol. Spectrosc., 54, 200
Endres C., Müller H., Brünken S., Paveliev D., Giesen T., Schlemmer S., Lewen F., 2006, J. Mol. Struct., 795, 242
Endres C. P., Schlemmer S., Schilke P., Stutzki J., Müller H. S. P., 2016, J. Mol. Spectrosc., 327, 95
Fletcher L. N., Greathouse T., Orton G., Irwin P., Mousis O., Sinclair J., Giles R., 2014, Icarus, 238, 170
Furtenbacher T., Császár A. G., Tennyson J., 2007, J. Mol. Spectrosc., 245, 115
Fusina L., Di Lonardo G., Johns J., Halonen L., 1988, J. Mol. Spectrosc., 127, 240
Gamache R. R., Vispoel B., Tennyson J., Yurchenko S. N., Polyansky O. L., Gordon I. E., Hargreaves R. J., Huang X., 2025, J. Quant. Spectrosc. Radiat. Transf., 345, 109568
Gordon I. E. et al., 2022, J. Quant. Spectrosc. Radiat. Transf., 277, 107949
Halonen M., Halonen L., 2006, J. Phys. Chem. A, 110, 7554
Hougen J. T., Bunker P. R., Johns J. W. C., 1970, J. Mol. Spectrosc., 34, 136
Job V., Kartha S., Kartha V., Thakur K., 1986, J. Mol. Spectrosc., 120, 205
Job V., Kartha S., Singh K., Kartha V., 1987, J. Mol. Spectrosc., 126, 290
Kartha S., Singh K., Job V., Kartha V., 1988, J. Mol. Spectrosc., 129, 86
Kelly M. J., Francke R. E., Feld M. S., 1970, J. Chem. Phys., 53, 2979
Lichtenstein M., Gallagher J., Derr V., 1964, J. Mol. Spectrosc., 12, 87
McKemmish L. K., Bowesman C. A., Kefala K., Perri A. N., Syme A. M., Yurchenko S. N., Tennyson J., 2024, RAS Tech. Instrum., 3, 565
Melosso M., Dore L., Gauss J., Puzzarini C., 2020, J. Mol. Spectrosc., 370, 111291
Melosso M. et al., 2021, J. Mol. Spectrosc., 377, 111431
Noumeroff B., 1923, Méthode Nouvelle de la Détermination des Orbites et le Calcul des Éphémérides en Tenant Compte des Perturbations. Gosudarsvennoe Izdatel'stvo, Moscow, p. 188
Olberg M., Bester M., Rau G., Pauls T., Winnewisser G., Johansson L. E. B., Hjalmarson A., 1985, A&A, 142, L1
Pavlenko Y. V., Yurchenko S. N., Tennyson J., 2020, A&A, 633, A52
Rodriguez Kuiper E. N., Zuckerman B., Kuiper T. B. H., 1978, ApJ, 219, L49
Roueff E., Lis D. C., Van Der Tak F. F. S., Gerin M., Goldsmith P. F., 2005, A&A, 438, 585
Shah R. Y., Wootten A., 2001, ApJ, 554, 933
Snels M., Hollenstein H., Quack M., 2003, J. Chem. Phys., 119, 7893
Snels M., Hollenstein H., Quack M., 2006a, J. Chem. Phys., 125, 194319
Snels M., Hollenstein H., Quack M., 2006b, J. Mol. Spectrosc., 237, 143
Sørensen G. O., 1979, in Dewar M. J. S. et al., eds, Large Amplitude Motion in Molecules II. Springer-Verlag, Berlin, p. 97
Tamassia F., Lonardo G. D., Fusina L., Canè E., 2025, J. Quant. Spectrosc. Radiat. Transf., 342, 109497
Tennyson J., Yurchenko S. N., 2012, MNRAS, 425, 21
Tennyson J., Hill C., Yurchenko S. N., 2013, in Gillaspy J. D., Wiese W. L., Podpaly Y. A., eds, AIP Conf. Proc. Vol. 1545, Eighth International Conference on Atomic and Molecular Data and their Applications: ICAMDATA-2012. Am. Inst. Phys., New York, p. 186
Tennyson J., Furtenbacher T., Yurchenko S. N., Császár A. G., 2024a, J. Quant. Spectrosc. Radiat. Transf., 316, 108902
Tennyson J. et al., 2024b, J. Quant. Spectrosc. Radiat. Transf., 326, 109083
Tiné S., Roueff E., Falgarone E., Gerin M., Pineau des Forêts G., 2000, A&A, 356, 1039
Walmsley C. M., Hermsen W., Henkel C., Mauersberger R., Wilson T. L., 1987, A&A, 172, 311
Weiss M. T., Strandberg M. W. P., 1951, Phys. Rev., 83, 567
Yurchenko S., 2023, Computational Spectroscopy of Polyatomic Molecules. CRC Press, Boca Raton, FL
Yurchenko S. N., Carvajal M., Jensen P., Lin H., Zheng J. J., Thiel W., 2005, Mol. Phys., 103, 359
Yurchenko S. N., Thiel W., Jensen P., 2007, J. Mol. Spectrosc., 245, 126
Yurchenko S. N., Yachmenev A., Ovsyannikov R. I., 2017, J. Chem. Theory Comput., 13, 4368
Yurchenko S. N. et al., 2024, MNRAS, 533, 3442
Zuckerman B., Ball J. A., Gottlieb C. A., 1971, ApJ, 163, L41

SUPPORTING INFORMATION

Supplementary data are available at *MNRAS* online.

ND2H-MarvelEnergies
ND2H-Transitions
NH2D-MarvelEnergies
NH2D-Transitions
readme
Segments-ND2H
Segments-NH2D

Please note: Oxford University Press is not responsible for the content or functionality of any supporting materials supplied by the authors. Any queries (other than missing material) should be directed to the corresponding author for the article.

This paper has been typeset from a TEX/LATEX file prepared by the author.